Environ Earth Sci
DOI 10.1007/s12665-009-0320-1

ORIGINAL ARTICLE

Coastal aquifer assessment based on geological and geophysical survey, northwestern Crete, Greece

Pantelis M. Soupios · Despina Kalisperi · Asimina Kanta · Maria Kouli · Pavel Barsukov · Filippos Vallianatos

Received: 23 February 2009 / Accepted: 3 October 2009

Abstract Groundwater preservation comprises a major problem in water policy. The comprehension of the groundwater/hydraulic systems can provide the means to approach this problem. Generally, drilling is expensive and time-consuming. On the other hand, new techniques have been applied during the last few decades that provide useful information on the depth and quality of aquifers. Among them, transient electromagnetic method (TEM) is an appealing method that provides fast results with minimum field crew and solves several hydrogeological problems. Many portable systems for single-site measurements are commercially available. The TEM-Fast 48HPC was used for acquiring 106 soundings in the northwestern Crete in Greece for defining the hydrogeological characteristics of the study area, since there were no available data from boreholes. Detailed geological, hydrolithological and tectonic survey was applied prior to the geophysical measurements. All the data were integrated to produce a secure and reliable hydrogeological model for the study area prior to any future hydrowell. Specifically, geometrical and hydraulic data of the study area groundwater were acquired. Two unconnected aquifers were detected and their possible contamination due to saltwater intrusion was analyzed and eliminated. Moreover, a location for borehole construction and groundwater pumping based on the potential of the aquifer system was proposed. Finally, the contribution of TEM (and electrical resistivity tomography) geophysical methods in studying complex coastal aquifers is shown by this work.

Keywords Water management · Hydrogeophysics · TEM · ERT · Hydrogeology · Coastal aquifer

P. M. Soupios (✉) · M. Kouli · F. Vallianatos
Laboratory of Geophysics and Seismology,
Technological Educational Institute of Crete,
3 Romanou, Chalepa, 73133 Chania, Crete, Greece
e-mail: soupios@chania.teicrete.gr

D. Kalisperi
Institute for the Environment, Brunel University,
Uxbridge, UK

A. Kanta
School of Earth and Environmental Sciences,
University of Portsmouth, Portsmouth, UK

P. Barsukov
Geoelectromagnetic Research Centre IPE RAS,
Russian Academy of Sciences, Moscow, Russia

P. M. Soupios
Department of Geophysical Engineering,
Faculty of Engineering, Ankara University, Ankara, Turkey

Introduction

Groundwater is one of the most important natural resources that sustains life on earth. The enormous and sudden expansion of industrial and agricultural activities has led to a quantitative and qualitative environmental degradation of the aquifer systems. Moreover, the most densely populated regions, all over the world, are located along the coastlines since they normally provide the best conditions for both economical development (low relief with high agricultural activities, commerce development, etc.) and quality of life. On the other hand, these regions suffer more than other areas from natural disasters as well as from scarcity of fresh groundwater due to seawater intrusion.

The groundwater contamination due to seawater intrusion is usually caused by a violation of a sensitive hydrogeological balance that exists between freshwater and seawater in coastal aquifers. This dynamic balance is

Published online: 20 October 2009

subverted by groundwater over-pumping and other human activities (e.g., land drainage) that lower groundwater levels and cause seawater movement into the coastal aquifers. It is obvious that the problem is important in all coastal aquifers, but it becomes vital in cases where the climate is arid and semi-arid, the precipitations are limited and the groundwater is inadequate since the rainfall is the only source of freshwater.

To rationally manage groundwater resources in coastal aquifers, where hydrogeological conditions are particularly dynamic and complex due to tectonic and other geological factors, a great amount of information regarding the geometrical and hydraulic properties of the aquifer is necessary. Most of this information is provided by observation and pumping wells; however, due to their scarcity and inevitably very local character of the information they provide, the supplementary cost-effective, non-invasive geophysical methods can provide continuous subsurface structural information to help geological mapping or geoenvironmental investigations, and their application is crucial.

The geophysical techniques offer a suitable method for determining the hydraulic and geometrical characteristics of an aquifer, since costs are reduced and results are good compared to the construction of a hydrowell, in which the final results are uncertain. Among all geophysical techniques (gravity, GPR, magnetics, resistivity, seismic refraction, etc.), electromagnetic methods are undoubtedly the leading ones in the exploration and management of groundwater. The most successful applications of the methods reported in the literature focus mainly on the studies of geometrical features of different geohydrological targets such as the configuration of fresh–saline groundwater interface, the thickness of an aquifer, of alluvial fill and gravel lenses over bedrock, the thickness and depth of sand and gravel lenses in till, etc. (Goldman et al. 1991, 1994b; Albouy et al. 2001; Kafri and Goldman 2005; Fitterman and Labson 2005; Barsukov et al. 2007; Chalikakis et al. 2008).

The transient electromagnetic (TEM) method has been used worldwide for hydrogeological surveys since several theoretical studies on the applicability of the method for groundwater investigation were undertaken. The TEM method is a fast and cost-effective method for exploring the subsurface and is of interest in this work. In the last decade, many scientists used the TEM method to solve hydrogeological and environmental problems, since the method was fully updated. Specifically, recent advances in digital technology have led to more innovative TEM instrumentations (e.g., TEM-Fast 48, DIALOG. http://www.aemr.net/ from AEMR, Geonics PROTEM47, Sirotem Mk3, ARTEMIS, Zonge NanoTEM) with improved capabilities for reconstructing the subsurface (from 10 m till 200 m underneath the surface) at areas where it was not always possible to deploy other geophysical methods. Moreover, the development of novel schemes for processing of the acquired TEM data can provide geologically (realistic interpretive model) two- and three-dimensional resistivity models without much reliance on the availability of a priori subsurface information (Christensen 1995; Meju 1996, 1998; Meju et al. 1999; Nielsen et al. 2007; Duque et al. 2008).

This paper describes a recent evaluation study of the applicability of a simple, fast, robust, portable TEM system, the TEM-Fast 48HPC developed by AEMR Ltd., using single loop 50 m × 50 m (coincident loop) for shallow-depth hydrogeological mapping in a near coast area in northwestern part of Crete Island, Greece. A total of 256 soundings in 106 different locations were acquired with different acquisition parameters for deeper penetration and better resolution. Prior to the geophysical work, detailed geological and tectonic mapping was accomplished and all the available information was used to construct a GIS platform. The problem in this study was that no prior information from boreholes in the study area was available for calibrating our results.

In short, the main aims of this study were the following: (a) to create preliminary hydrogeological/geophysical expectation models for the study area, (b) to combine the geological, tectonic, hydrolithological, geophysical and other information to generate scenarios that could provide answers to the key hydrogeological questions developed for the area under investigation, (c) to establish the depth, thickness and other characteristics of the study aquifer, (d) to upgrade and re-interpret the hydrogeological expectation model based on the final 2D and 3D geophysical models, and (e) to identify a high-potential groundwater target area based on available groundwater information for the construction of pumping well for the groundwater.

General hydrogeological knowledge

Description of the area

The study area is situated in the northwestern part of the Chania Prefecture. The total area is 5.4 km^2 and is about 12 km east of Chania city. Geographically, the study area is defined by the villages, M. Horafia and Aptera, which are included in the area under investigation, the Malaxa village to the west, the Kalyves village to the east, the Stylos village to the southeast and the coastal line to the north (Fig. 1).

The topography of the study area is quite smooth with gentle to moderate slope, while the highest survey point reaches an elevation of 240-m above sea level (masl). The place is a tourist spot and near Chania city, the airport and the port of Chania municipality. As much as 500 people live in the study area, while the population increases three

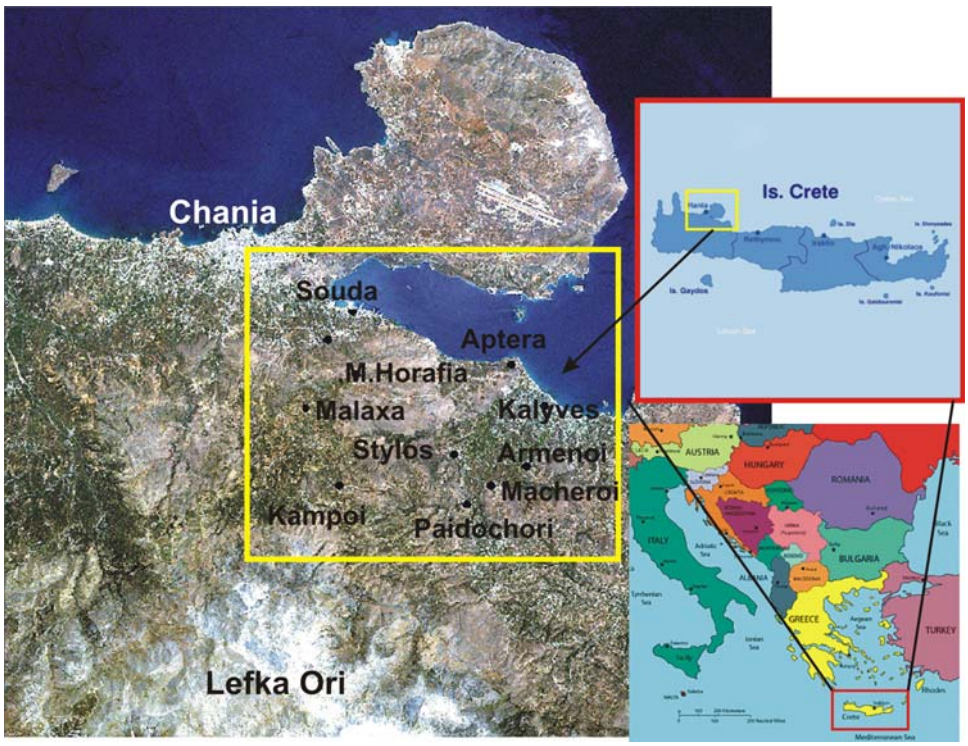

Fig. 1 The maps show the study area in different scales. The *yellow rectangle* defines the borders of the broader area under investigation

times more during the summer period. This shows the increasing needs of potable and irrigated water for the further development of the area.

Geological, tectonic and hydrogeological settings

The broader area is composed of the following geological units (Table 1) (Papanikolaou and Vassilakis 2008): (1) loose Quaternary (Q_2–Q_1) deposits (alluvial deposits, terra rossa, clays and weathered materials from the erosion of calcitic rocks), (2) Neogene (N_2–N_1) deposits (mainly consists of marly limestones, marls, sandstones and clays), (3) the Tripolis (T_3–K_2) geotectonic zone (Tripolis nappe–Upper Triassic to Cretaceous) consisting of marls, marly limestones, limestones and dolomites fractured and folded (4) arna nappe (Paleozoic) in Permian period flysch and metamorphic rocks (P–T_3) (phyllites, quartzites, shales, schists and meta-sandstones), (5) western crete nappe of Trypali Carbonates-unit (T_3–J_1) (Late Triassic–Early Jurassic), which is composed of cohesive limestones and dolomitic limestones in the deeper part and calcitic breccias and conglomerates at the shallower part of the unit, and (6) the autochton Mani carbonate sequence (J_1–E_2) (between Early Liassic and Eocene, Kocka et al. 2007) consisting of Plattenkalk, dolomites and undivided carbonated formations. Specifically, as presented in the geological map of Fig. 2, the study area is occupied by: the Quaternary (Q), Neogene (N) and Trypolis formations (T_3–K_2).

During the fieldwork, 15 fracture zones were identified, evaluated and recorded in the study area, using of course previous geological studies as well. The majority of the tectonic lines have N–S direction as shown in Fig. 2, three tectonic lines follow the NE–SW direction and two E–W tectonic lines were also recorded that form the horst where the M. Horafia and Aptera villages are located. It can also be observed that the river network follows, in some cases, the direction of the major tectonic lines as was expected (Tucker and Bras 1998). There are preparatory and triggering causal factors of groundwater contamination in the study area besides the type of the geological and hydrolithological formations. Some of them are the extensive tectonic fragmentation in different directions; the intense morphological relief with the steep slopes (where limestone is outcropped) and the over-exploitation of existing hydrowells (in the eastern southern part of the area) due to human activities (near Stylos village).

During the geological mapping, and in collaboration with a geologist from the local water management authorities (Dr. K. Vozinakis from the Water Management Authority of Chania Prefecture), a borehole contaminated with high chlorine concentration (high conductivity in geophysical measurements), in the area that was included in the ellipse (Fig. 3), was notified. The areas that were contaminated (ellipses in Fig. 3) by saltwater intrusion were about 6–20 m above the sea level (masl), as shown in Fig. 3, and all geophysical measurements were acquired on a plateau with a mean elevation of about 160–170 masl.

Table 1 The nappe pile of Crete (modified from Fassoulas et al. 1994). The third (3rd) and fourth (4th) column of the table present the age and the hydrolithological characteristics of the formations, respectively

Post-Alpine rocks	Quaternary deposits	Q_2–Q_1	P1
	Neogene deposits	N_2–N_1	P2, P3
Alpine and pre-Alpine rocks	Upper nappes		
	Ophiolites		
	Asteroussia nappe		
	Tectonic mélange		
	Pindos nappe		
	Tripolis nappe	K_2, J_3–K_1, T_3–J_2, T_2–T_3, $\mathbf{T_3}$–$\mathbf{K_2}$	**K1**
	Lower nappes		
	Phyllite-Quartzite nappe	**P–T_3**	**I2**
	Trypali nappe (Western Crete)	T_3–J_1	
	Ionion nappe (Plattenkalk series)	T_3, **J_1–E_2**	**I2**

The information depicted in bold represents that formations were found in the broader study area

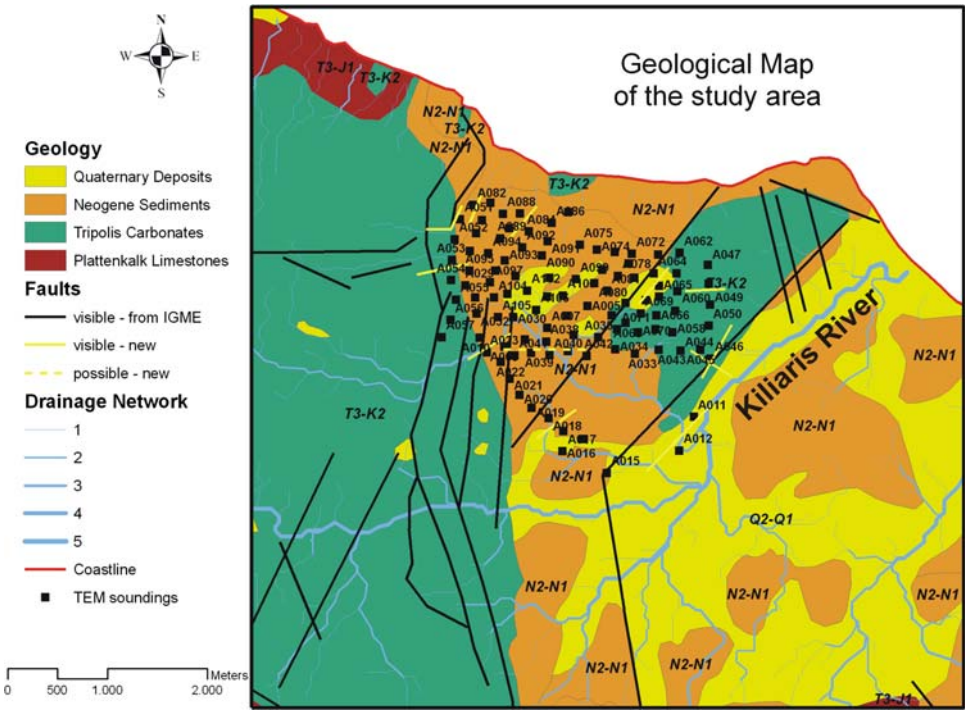

Fig. 2 The revised geological map is presented including some information about the tectonic regime of the area and the river network (Kiliaris river) as extracted by the DEM's processing. The *black* and *yellow lines* indicate the tectonic lines that are found and verified by the IGME (Institute of Geology and Mineral Exploration of Greece) maps and during the fieldwork, respectively. The location of the TEM soundings (*black filled rectangles*) are also presented

From the hydrolithological point of view, the geological formations are classified into five hydro-lithological units: (a) (**K1**) high to medium permeability rocks, which comprise the karstic limestones of Tripolis and Trypalion nappes and dolomitic rocks. Water movement is accomplished through the fracture zones and the chaotic karstic system (secondary porosity). A high groundwater potential is expected and usually discharged by means of karstic springs (Figs. 3, 4); (b) (**P1**) fluctuant permeability formations, which are composed of recent to present alluvial deposits, eluvial mantle materials, fluvial deposits, talus cones, dunes and conglomerates in places. A shallow and low-potential aquifer is expected and is of interest to ecosystem studies because of its interaction with surface water flows; (c) (**P2**) medium to low permeability formations, which consist mainly of Miocene and Pliocene deposits (Neogene marly limestones and conglomerates); (d) (**P3**) low to very low permeability formations, which are composed of Pliocene and Miocene marls and other impermeable Neogene formations; and (e) (**I2**) low to very low permeability formations, which are mainly composed of metamorphic (phyllites, etc.) and rocks of all the geological units and nappes (including the Ionion nappe). In some cases, depending on the fracturing or the composition

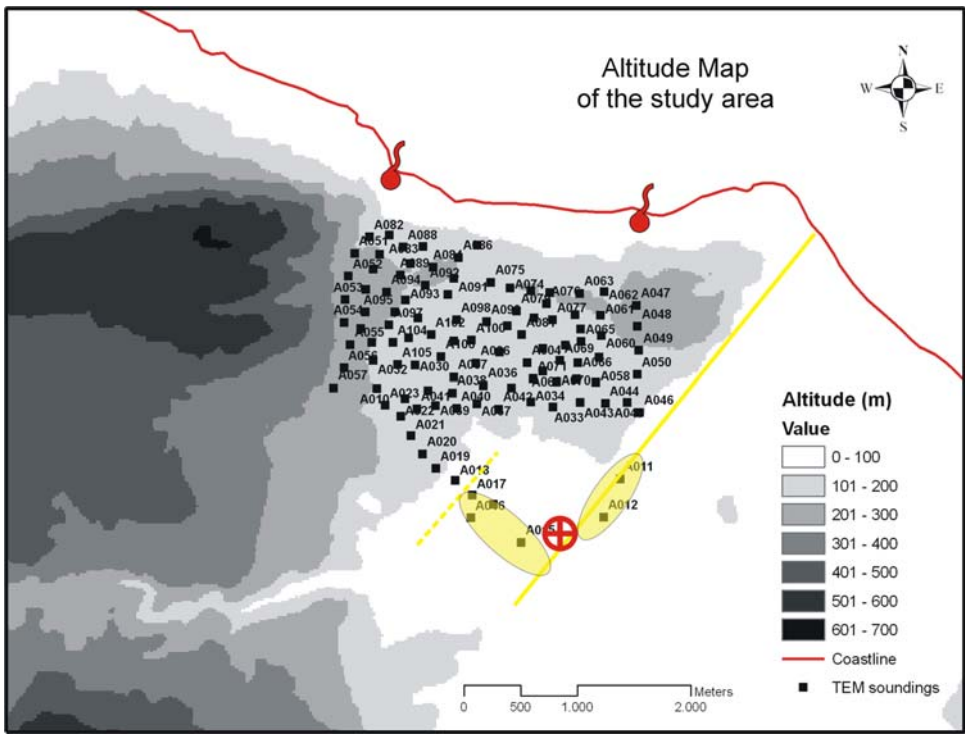

Fig. 3 The altitude map of the broader study area is shown as produced by processing the digital elevation model of the area under investigation. The *filled rectangles* show the location of the TEM soundings. The *yellow lines* depict two parallel NE–SW tectonic zones (*continuous* for defined and *dashed* for possible). The *ellipses* show areas of shallow aquifer with high conductivity (contaminated with saltwater intrusion), and at the southeast of the study area, the *red geological symbol* presents the location of the contaminated (high Cl^{-}) hydrowell. The two *red symbols* along the coastline depict the location of the two karstic springs

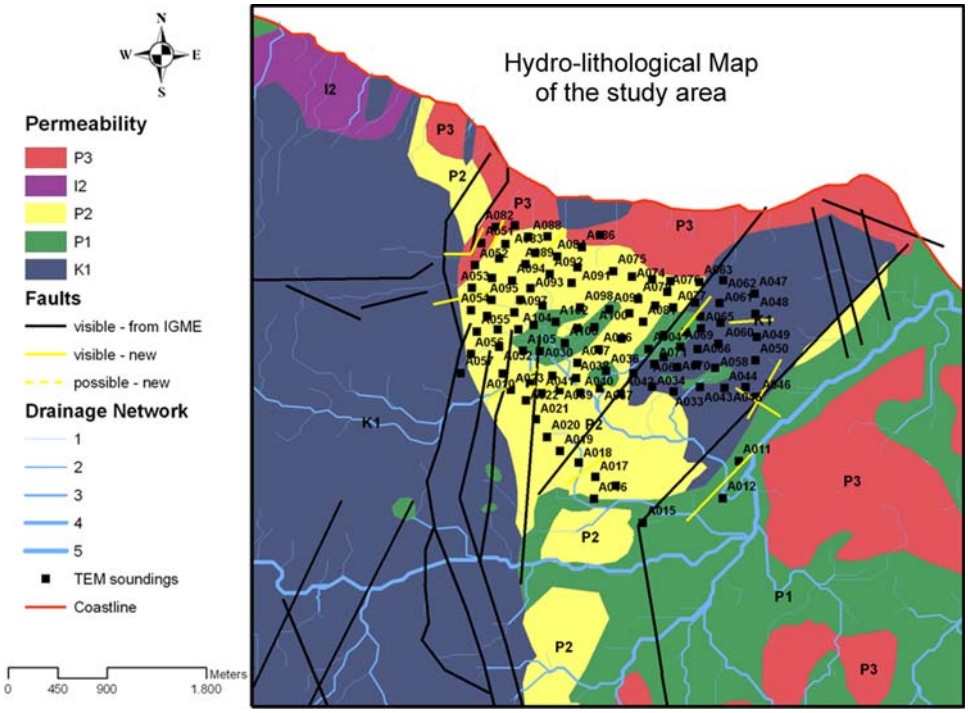

Fig. 4 A hydrolithological map, produced by classification of the geological formations (Fig. 2) based on permeability, is presented. Five units are depicted (P3, I2, P2, P1 and K1) and described into the text ("Geological, tectonic and hydrogeological settings"). All the recognizable fracture zones (*black* and *yellow lines*), the river network (based on Strahler's system classification, 1–5), the location of the TEM soundings (*black filled rectangles*) and the location of the karstic springs (*yellow geological symbols*) are presented

(alternation of quartzites and marbles), high-potential aquifers can be found.

The flow of surface water in the broader area comes from the mountainous area (Lefka Ori) on the south-western part of the study area. The main river (Kiliaris River), shown in the eastern part of the area (Fig. 2), drains into the valley, but the flow is essentially blocked by the slight rise in elevation along the coastline. The tectonic regime of the area, the different flow regimes and the general hydrogeologic and hydrolithologic framework affect the pattern of seawater intrusion and recharge.

Climatic–land use data

The average annual precipitation (which is mainly the recharge source of the aquifers) is estimated to be 900 mm (Chartzoulakis et al. 2001). Crete is a semi-arid region with humid and relatively cold winters and dry and warm summers. During winter that starts usually in November, the weather is unstable due to frequent changes from low to high pressure. The annual rainfall for the broader Chania area has been estimated to be 665 mm. That number was approximately calculated as the total yearly precipitation on the plains. About 65% is lost to evapotranspiration, 21% as runoff to sea and only 14% goes to recharging the groundwater (Chartzoulakis et al. 2001). The rainfall is not uniformly distributed throughout the year, and it is mainly concentrated in the winter months, while the drought period extends over more than 6 months (May–October) with evaporation values ranging from 140 mm to more than 310 mm in the peak month (during July) (Tsagarakis et al. 2004). This non-uniform distribution of rainfall causes several problems to the water management authorities, since there is a long dry summer period during the peak tourist season. Finally, the land use of the study area is mainly agricultural (up to 80%), pasture coverage is up to 10% and the natural vegetation coverage represents less than the 10%.

Data preparation in GIS platform

To create the appropriate information platform on which to proceed in a systematic way toward applying the water management models through the use of geological and geophysical data, all available data in the form of maps were used as the basis for the creation of GIS thematic layers.

The data pre-processing involved their implementation into a GIS environment. Several maps were geo-referenced to the local projection system of Greece (GGRS'87: Greek Geodetic Reference System) so that they could all be tied to the same projection system, together with all future information that may become available. In the next pre-processing phase, digitization of all the relevant data maps, namely lithological, structural and topographical, was carried out. The Digital Elevation Model (DEM) of the study area with a cell size of 4 m is a continuous raster layer, in which data values represent elevation. The DEM was generated from the topographic maps of the study area. The lithology layer was derived through the digitization of the published geological maps, which display major rock groups and structural features. The drainage network was automatically extracted from the DEM and the drainage tributaries (Fig. 4) were then classified according to the Strahler's system (Strahler 1964).

Geophysical method used

The TEM method has been used in environmental and hydrogeologic studies over the last 15 years. A detailed description of the method is given by Danielsen et al. (2003) and belongs to the category of controlled source EM methods. The TEM method makes use of a direct current transmitted into the transmitter loop lying on the ground. The current creates a primary, stationary magnetic field. The direct current is switched off, which induces an eddy current system in the ground. Due to ohmic resistance of the subsurface, the current system will decay and further induce a secondary magnetic field that is measured in an induction coil (the receiver coil). The decay rate of the electromagnetic field depends on the resistivity distribution of the subsurface. The field decay is slower in a conductive rather than in a resistive medium.

The importance of the TEM method lies on the measurement time of the transient response. As already mentioned, the induced voltage at Rx (Receiver) loop is measured after the turn-off of the Tx (Transmitter) loop. That means that we measure a secondary response in the absence of the primary field. This approach produces results less sensitive to errors of Tx/Rx geometry, there is no need for complicated tools to separate the primary signal and, finally, the Tx/Rx separation has a small effect in the exploration depth (in contrary to conventional controlled source methods). These features produce results with the highest lateral resolution.

Consequently, the TEM method has excellent resolution of conductive layers at depth, whereas the resolution of resistive layers is limited (Christensen and Sørensen 1998). TEM soundings are usually made with loop size ranging between 150 and 250 m, depending on the exploration target. The penetration depth is dependent on the magnetic moment of the equipment (i.e., transmitter loop size and number of turns and the transmitted current), the resistivity of the ground and the magnitude of electromagnetic background noise (Macnae et al. 1984; McCracken et al. 1986).

Advantages of the TEM method are its sensitivity to conductors at great depths and the lightweight equipment compared to other geophysical methods. Drawbacks of the TEM method are low resolution of resistive layers and high degree of coupling to man-made conductors.

Data acquisition: processing

All the data (geological mapping and geophysical survey) were collected in 45 days. In total, 256 TEM soundings were acquired in 106 different locations (Figs. 2, 3, 4). The measurements were carried out in a detailed survey grid (about 100–150 m in X and Y dimensions) to be able to

image a possible complex (3D or due to the tectonic) subsurface. During the geophysical fieldwork, the team was very careful about the optimum site selection, the installation of the antenna and other environmental conditions, which can produce noisy and bad quality data. The root mean square (rms) error of the final data set was less than 7% (between 0.45 and 7%).

A single turn, 50 m × 50 m single loop setup was used to gain sufficient penetration depth. The system was set to transmit current up to 4 A with 32 active time gates from 4 to 1,024 μs and a stacking time of about 3 min. To define and avoid aliasing effects (high-frequency (HF) noise from radio sources), the measurements were repeated several times at each sounding location.

The processed data produce a 1D resistivity model with depth. Based on the international bibliography and depending on the geological conditions of the study area, resistivities greater than 10 ohm m usually result from the presence of freshwater in the subsurface and resistivity less than 10 ohm m indicate the existence of brackish/contaminated water (Alsharhan et al. 1998).

The collected data were processed after the acquisition providing the one-dimensional (1D) distribution of resistivity with depth. The TEM-RESearcher, a Windows-integrated software system, was the tool for data processing of TEM data and inverse problem solution. The aforementioned program is a user-friendly tool that is convenient for TEM data editing, smoothing, analysis and processing. Geoelectric sections (2D pseudo-sections) and depth slices (resistivity and conductivity maps) are easy to be constructed in the class of gradient or layered structures (TEM-RESearcher manual 2007).

Generally, 1D modeling is inadequate to describe 3D subsurface structures. Presently, several works, e.g., Newman et al. (1987), Goldman et al. (1994a), Auken (1995) and Hördt and Scholl (2004), show that if the geological condition consists of smoothly varying 3D structures with moderate resistivity contrasts, the 1D inversion approach gives a satisfactory reconstruction of the true model. Of course, in case of high-resistivity geological contacts and/or contrast and strong 3D features, an 1D approximation is strongly influenced by 3D effects and in many cases will provide unreliable models.

Interpretation: results

1D interpretation

As mentioned above, TEM soundings are commonly used to define aquifer properties and other subsurface characteristics. Of course, those kinds of structures are multi-dimensional, but 1D inversions are used to determine geologic structure for groundwater flow models. Generally, they can be imaged without big errors.

Figure 5a and b show an example for the A012A TEM sounding. All field (raw) data were "edited" (e.g., first points were excluded from the curve for further analysis) and "smoothed" before modeling, as the manufacturer suggested (Barsukov et al. 2007) (Fig. 5a). TEM-RES software provides two ways of construction of a section,

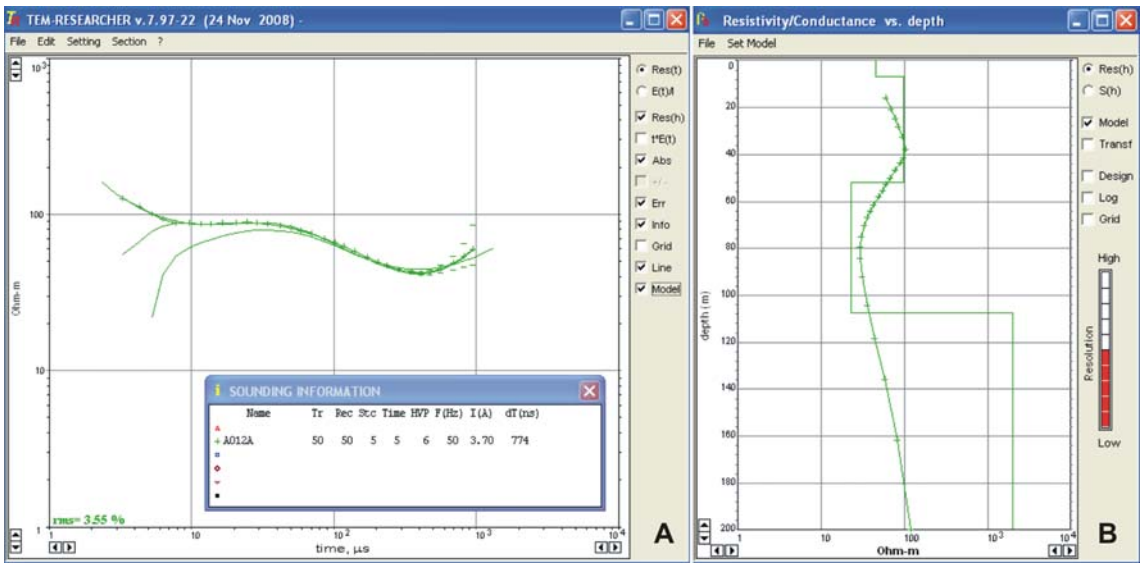

Fig. 5 **a** Curve of apparent resistivity $\rho_a(t)$ (example of sounding A012A). Two more curves are given as a result of the raw data smoothing. The first (*upper*) continuous curve approximates initial $\rho_a(t)$ data and the second (*lower*) curve is the calculated dependence $\rho_{full}(t)$, **b** The transformation ($\rho(h)$) and inversion (example of sounding A012A) are presented by the smooth curve and the piecewise uniform diagram, respectively. For details see text (section "Interpretation: results")

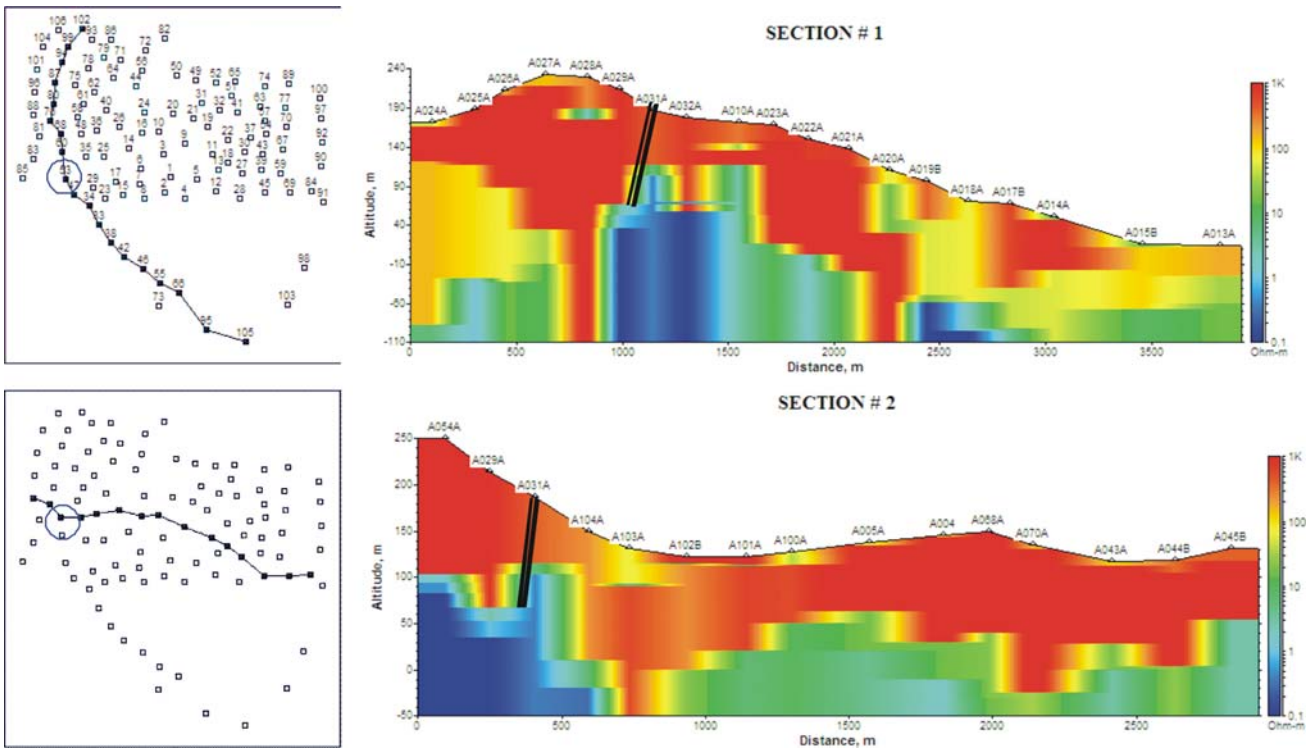

Fig. 6 Two-dimensional representation of the resistivity distribution in depth are given for a NW–SE and W–E profiles. The suggested location for the construction of a hydrowell is presented by the *double black lines* at sounding A031A

transformation and inversion. Figure 5b shows the transformation Res(h), which is distribution of specific resistivity versus apparent depth (smooth curve) and the model after 1D inversion (piecewise uniform diagram).

2D interpretation

Since the 1D modeling is inadequate to reconstruct and describe the subsurface, 2D imaging is required. TEM-RES software is a great tool for the construction of geoelectrical sections as well. So, the 1D inversion data are received and the user can choose any profile that prefers to illustrate. In Fig. 6, a NW–SE and a W–E sections are represented as tomography and it is a color presentation of the structure.

Hot (red) colors represent high-resistivity formations and the cold (blue) colors depict the low-resistivity units as well. The length of the first profile is 3,900 m and a low-resistivity area is depicted by the double black lines (Fig. 6). We assumed that this area is the main high-potential aquifer. Similar results were acquired from the interpretation of the second profile. In the same cross section sounding (A031), a promising aquifer zone is detected from a depth of 80 m below the surface. Detailed study of this groundwater resource will be presented in the following section "Discussion".

To show the applicability of the TEM method for mapping of subsurface and for determining the hydrogeological regime of the study area, one more 2D profile in the direction of W–E is presented in Fig. 7 in comparison with the geological section. As shown, at the western and eastern part of the profile, the limestones (T–K) were detected, but the geophysical interpretation was not the optimum since the signal was very noisy (very resistive formations). The mapping in the central part of the profile is accurate and is in agreement with the geological formations of the area (Quaternary, Q and Neogene, N formations). The bedrock of the area under investigation is (as expected) the phylites–quartzites ($P–T_3$) formation as depicted in the figure given below. This finding is very important for this hydrogeological study, since the $P–T_3$ unit appears to show selective permeability due to the high distress and fracturing of this formation.

3D image: depth slices

The final 1D inverted models from all the available (good quality, free of noise) TEM data were topographically corrected (taking into account the real elevation of each measurement) and merged to form slices differentiated according to depth. The roof and the bottom of each layer

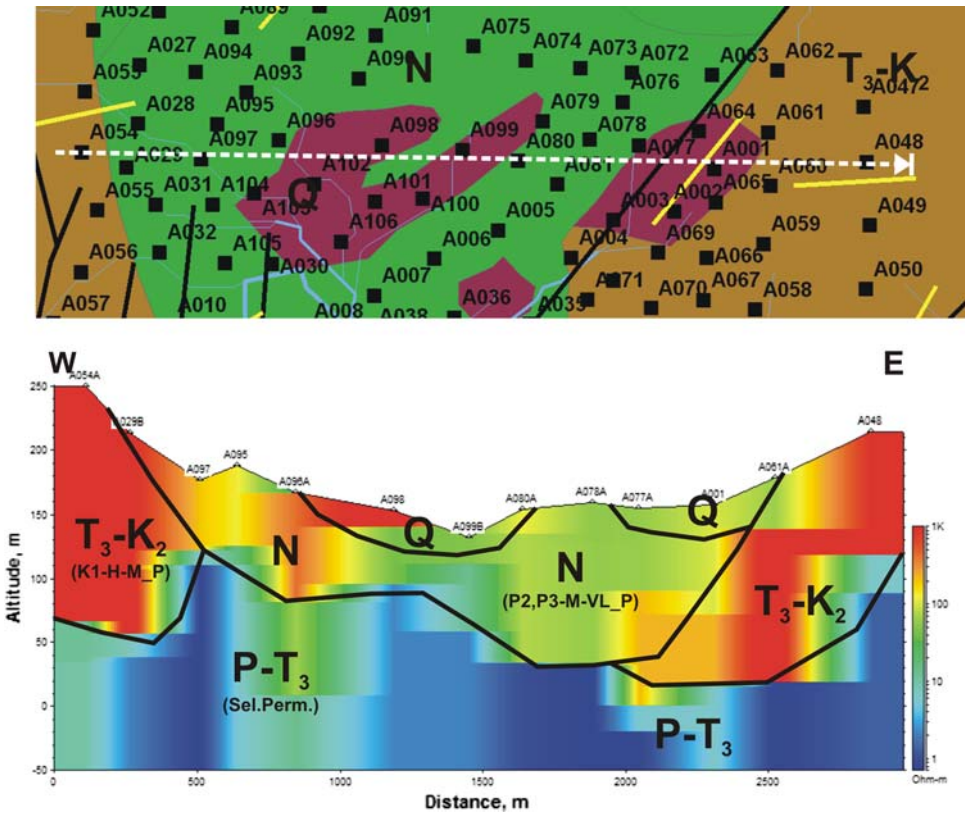

Fig. 7 The geophysical profile overlaid by the geological section is provided and presented for comparison and evaluation. The geophysical section that resulted from the interpolation of the 1D TEM data is in agreement with the geological section of the study area for the specific W–E profile. The permeability of the geological units is also provided. K1-H-M_P: K1 hydrolithological unit with high to medium permeability, P2, P3-M-VL_P: P2 and P3 hydrolithological units with medium to very low permeability and Sel.Perm: the impermeable bedrock with selective permeability based on fracturing

were defined prior to the creation. The positions of the soundings were also included in the final presented slices for controlling the coverage (resolution of the reconstructed model) of the area by the density of the measurements. The estimated model is represented as six different depth slices (Fig. 9) with depths 0.0–25.0, 25.0–50.0, 50.0–75.0, 75.0–100.0, 100.0–150.0 and 150.0–200.0 m, respectively.

Discussion

Questions to be answered

According to the above indicated hydrogeological assumptions and tectonic/geological data, the following questions should be answered prior to any borehole suggestion and construction.

1. Is there any possibility of contamination of our aquifer in the study area due to the proximity with groundwater contaminated by saltwater intrusion? (Stylos area: area A in Fig. 8). The TEM methods are capable of detecting an interface between a fresh groundwater body and an underlying saline one through the expected sharp drop of resistivities.
2. Could we detect any hydraulic connection between the contaminated region (area A) and our study area? Based on the tectonic data, the TEM depth slices and the geometric characteristics of the groundwater and specifically the real elevation of the roof and bottom of the aquifers, we can safely assume any possible interconnection between the areas. The base level change in the study and contaminated aquifer controls the fresh/saline water hydrodynamic system.
3. Can we determine from where the study area is recharged? The answer can be possibly "hide": governed by the tectonic characteristics of the area, in case where mountainous areas, which usually act as the recharge zone, are close to the area under investigation. The 3D resistivity imaging of the subsurface certainly helps to give answers.

The analysis (see below) of Figs. 8 and 9 will give answers to most of the aforementioned questions.

Analysis

The upper (shallower) slice (Figs. 8, 9) should be directly correlated with the surficial geology if the TEM interpretation was accurate. The hot (red) colors represent the high-resistivity formations (the Trypalion limestones) since the

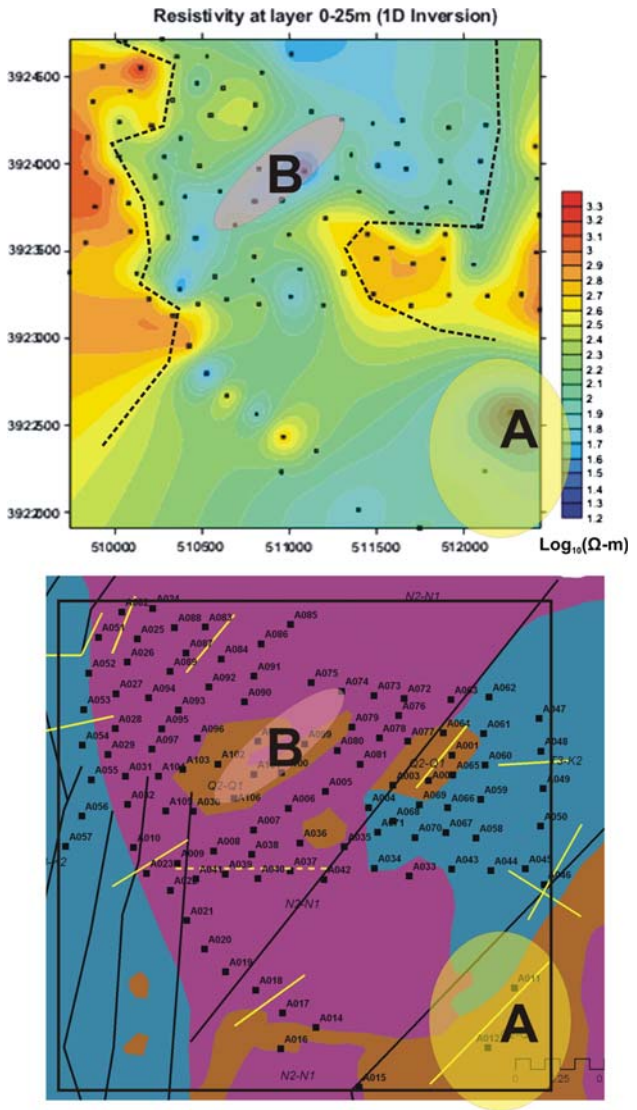

Fig. 8 Comparison between the shallower geophysical slice and the regional geologic field map is presented. Two low-resistivity areas are found (*A* and *B*), which correlate with saltwater intrusion and shallow aquifer, respectively. Based on the shape of the contact between the geophysical units, two fault zones are assumed and verified by the geological mapping

cold (blue) colors depict the Quaternary and Neogene formations. The limits between the different geophysical units (dashed lines) are clear and coincide with the geological borders (different colors) as shown in Fig. 8. Two low-resistivity areas (A and B) were depicted. The area A, which consists of three soundings, appeared with very low resistivity (about 0.1 ohm m). It was easy for the processing team to recognize the correlation between that area and the area with the contaminated (from seawater intrusion) borehole, which was mentioned above as a priori information. Area B, which consists of six soundings, shows low resistivity (less than 30 ohm m but greater than 10 ohm m) and can be safely correlated with the P1 hydrolithological unit (section "Geological, tectonic and hydrogeological settings"), which is characterized by shallow and low-potential aquifer. The appearance of the shallow (low potential) aquifer in area B was confirmed both by the locals and geological mapping, since several shafts were found, which were used to pump the groundwater during the winter period. The shape of the contact between the calcitic rocks and the Neogene formations in the eastern (SE of B anomaly) and in the western part of the area is sharp and considered to be the fault zones, trending approximately NE–SW (continuous line in Fig. 2) and almost WWN–EES (red line in Fig. 2), respectively.

Figure 9 shows the geophysical slices from the depth of 0 m till the total depth of 200 m. The first shallower slice had been discussed already. In the second depth slice (25–50 m), high and intermediate resistivities were met in the western and the eastern part covered by the calcitic rocks and in the central part covered by Neogene formations, respectively. The geological contact between the Trypalion limestones and the Neogene formation is depicted by thick dashed lines. The resulting resistivity map is in agreement with the regional geological field map (Fig. 8). At first, the sharp changes in resistivity inside the calcitic rock was assumed to be fracture zones, but finally it was verified after the interpretation, when the mapped tectonic features overlapped the depth slices. Thus, the thick red dashed lines, in the western part of the area, illustrate the almost E–W fracture zones that create the tectonic uplift (horst) where the M. Horafia and Aptera villages are situated.

In the third depth slice (50–75 m), high and intermediate/low resistivities are detected at the northern part of the model excluding the coastal area. The Trypalion limestones in the eastern part seem to be connected with the western part (the bedrock emerged creating the aforementioned horst) due to the E–W fracture zone (red thick dashed lines). Based on the geophysical interpretation, it can be assumed that the thickness of the Neogene formation is about 70–75 m. A shallow aquifer, which covers a small area, is detected at a depth of 60 m and is depicted in Fig. 9 by the transparent ellipse. This low-resistivity area continues till a depth of 200 m and expands covering the western–southern part of the model, having also some linear characteristics that should be explained.

Based on the current situation, the roof of the aquifer (at 60-m depth) is determined. Continuing the interpretation of the deeper slices (75–150 m), the resistivities are more homogeneous with some exceptions where the bedrock is still unsaturated (cohesive and unfractured bedrock). The elongated dashed lines show two tectonic zones that "isolate" the study aquifer system from the two neighboring contaminated areas, the northern part (the coastline) and the western–southern part (Stylos, Area A in Fig. 8). The north tectonic zone that has almost an E–W direction

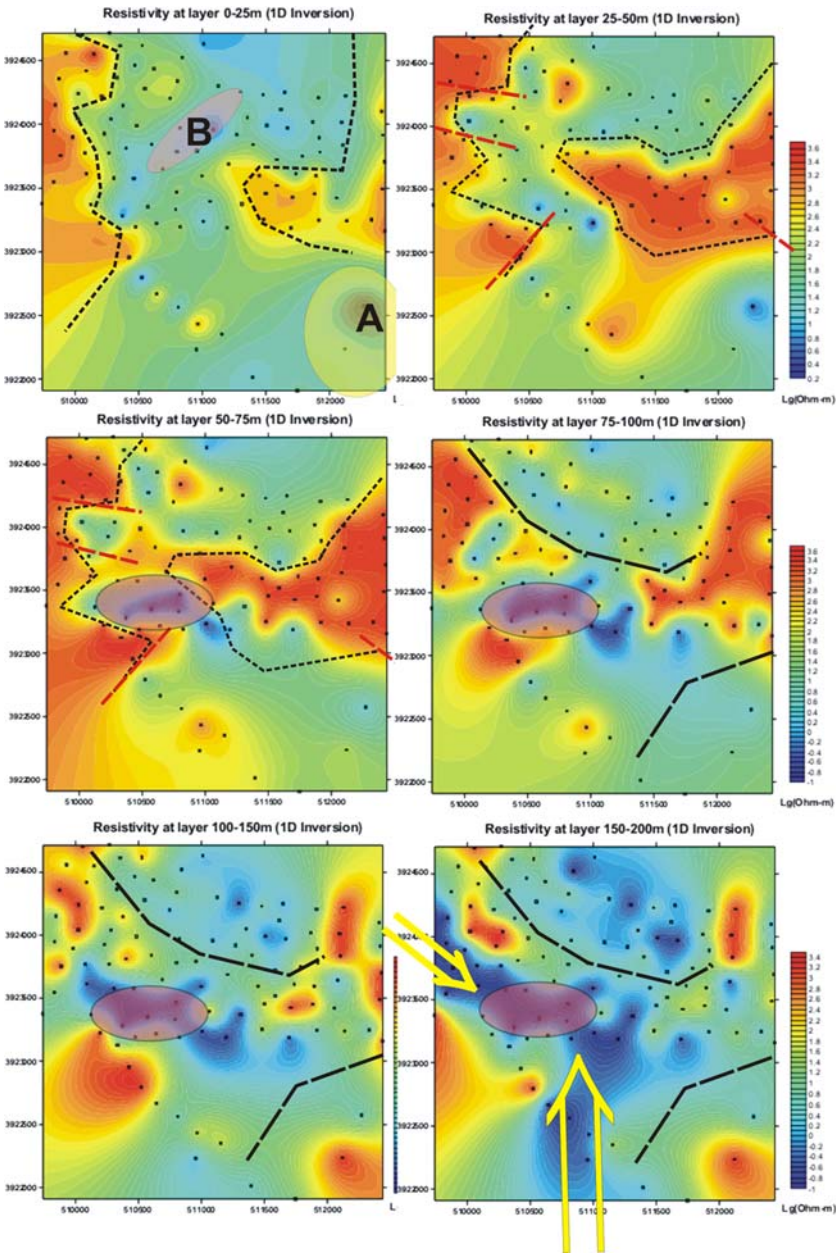

Fig. 9 The geoelectrical interpretation till a depth of 200 m is presented. *Red dashed lines* depict the observed fractures zones of the area. *Dashed lines* in the depths from 25 to 75 m define the limits of the high-resistivity geological calcitic formations, which are in agreement with the local geological map. The transparent ellipse from a depth of 50–200 m depict the study aquifer system. The *elongated dashed lines* presented from the depth of 75–200 m show and describe the "isolation" of our system from the neighboring contaminated regions (coastline and area *A*). *Yellow arrows* define the direction of the recharge of our aquifer system

was determined from the processing of the digital elevation model, but was also observable through the interpretation of the second resistivity slice. The second zone separates the measurements that were taken near the area A (011, 012, 014, 015 and 016) with average elevation of about 6 masl, from all the other measurements that were taken in a plateau with an average elevation of about 160–170 masl (see the altitude map—Fig. 3). Those lines define the survey area and provide answers to questions 1 and 2 of the working hypotheses.

Specifically, it seems that the aquifer is bounded from the northern side of the study area by the E–W tectonic zone and from the southwestern side by an NE–SW tectonic zone. From a depth of 100–200 m north of the dashed line, a conductive zone is observed that is correlated with the overflow springs defined in Figs. 3 and 4.

In Fig. 9 at the deepest slice (150–200 m), the directions of the recharge (yellow arrows) of the aquifer system are presented. The study aquifer system is recharged from the karstic mountain of Lefka Ori (2,600 m) from the south–southwest and from the Plattenkalk formation in the west. The study area is near the foothill of the mountains and the fracture zones play an important role for the water recharge of the study area since the groundwater moves through those zones as depicted in Fig. 9. This is the answer to question 3 of the working hypothesis about the recharge zone of the area under investigation!

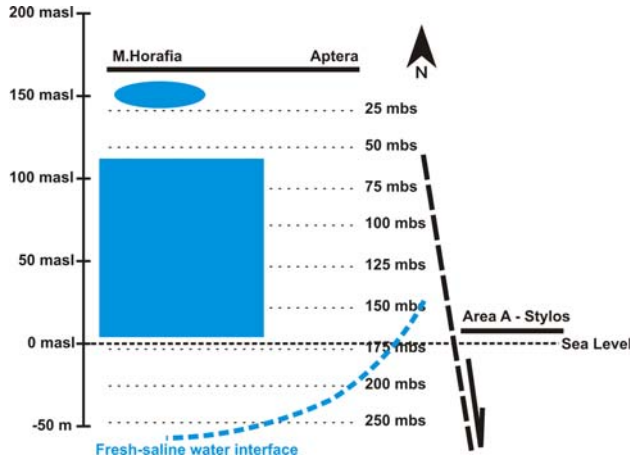

Fig. 10 A simplified, but informative, hydrogeological sketch of the resulting model for the study area is presented. The blue filled ellipse and rectangle define the shallow and deeper aquifer, respectively. The *Y*-axis depicts the difference in elevation (*masl* meters above sea level). The horizontal dotted lines define the depth in meters below the surface (mbs). The *thick*, *black dashed line* show the fracture zone that separates the two aquifer systems (our study area and the contaminated Area A, Stylos). The *blue dashed line* presents the parabolic interface between fresh–saline water according the Ghyben–Herzberg principle

Final simplified hydrogeological model

Consequently, a shallow and a deeper aquifer system were found (Fig. 10). The second and most important have the following geometrical characteristics. The depth (free water table) of the aquifer is 60–70 m (110–120 masl). The thickness of the system is about 120 m; thus, the bottom of the aquifer is determined to be 160–170 m deep from the surface (almost at the sea level). Note that the maximum depth of our geophysical investigation was 150–200 m. The aquifer covers an area of 0.56 km^2. The expected recharge can support a high-potential aquifer system.

As shown in Fig. 10, the area (A) near the Stylos village in which the groundwater contaminated by seawater intrusion has more than 150-m disparity in elevation from the plateau where all the measurements were taken. Also, a fracture zone exists between two areas as presented in the figure below. It is assumed that there is no contaminant movement from area A to the aquifer system since this fracture zone (based on geoelectrical measurements) acts as barrier to the water movement. Even if we presume that an interconnection between the two different qualities of water exists, under static and non-artesian conditions (simplest case), this should follow the fresh–saline water interface according to the 1-to-40 relation of the Ghyben–Herzberg principle (Drabbe and Ghyben Badon 1889; Herzberg 1901; Verruijt 1968).

A century ago, two hydrologists (Ghyben and Herzberg) working along Europe's coast observed that fresh groundwater, appearing to float as a lens-shaped body on seawater, extended below sea level approximately 40 times the height of the freshwater table above sea level. This 1-to-40 relation occurs because freshwater is slightly less dense than seawater (1.000 vs. 1.025 g/cm^3, respectively). Thus, for example, if the water table at a given site is 3 m above sea level, the freshwater–seawater transition zone is 120 m below sea level, and the vertical thickness of the freshwater body is 123 m. Based on this simple calculation, we can estimate that since the height of the water table above sea level is 100–120 m, the fresh water is still present deeply and there is no chance for seawater intrusion and contamination of the study system.

Based on all the extracted information from geological, hydrogeological, tectonic and geophysical study of the survey area, the optimum position for the construction of the hydrowell in the area is presented in Fig. 6 as the double black lines at the sounding A031. This sounding is included into the area of high-potential aquifer (ellipse of Fig. 9).

Verification of the resulting geoelectrical (TEM) structure

In many cases, the subsurface cannot be resolved into plane homogeneous layers, as required for a VES (vertical electrical sounding) or a TEM investigation, or into simple zones of lateral conductivity variation as required for profile interpretation. As a result, a combination of the two techniques is usually applied. ERT (Tsourlos and Ogilvy 1999; Stummer et al. 2004; Wilkinson et al. 2006; Tsourlos et al. 2006; Kemna et al. 2006; Athanasiou et al. 2007; Papadopoulos et al. 2006, 2007) is a usual and reliable approach to this problem. ERT profiles can be measured either in two dimensions, with the assumption that minor variation exists in bulk material values in the third (normally the *y*) dimension, or in three dimensions. Two-dimensional application is routine and the field and interpretation procedures have been developed to the extent that the process is now as rapid as the one-dimensional sounding investigation. Each electrode (all the combinations between the current and potential electrodes) is connected to a takeout on the multicore cable, which is connected to a manually or an automatically controlled switching box.

In this study, a geoelectrical resistivity tomography (ERT) was planned and implemented, as it was proved to be the appropriate geophysical method to model and verify the final 2D geophysical section (as extracted by interpolation of the 1D resistivity model) of the TEM measurements.

The geoelectrical data were collected using an IRIS-Syscal R1 Switch 48 instrument and the dipole–dipole

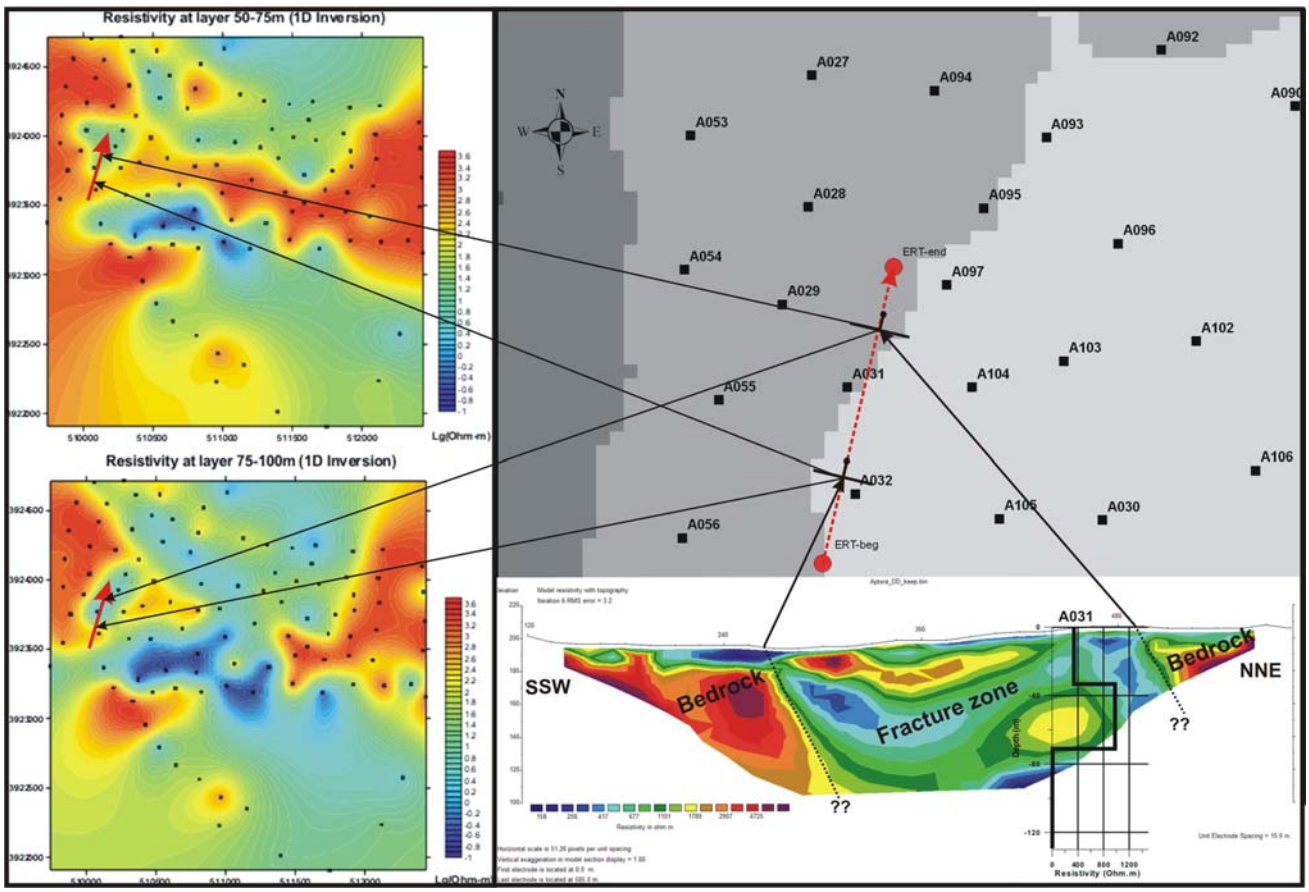

Fig. 11 Combined interpretation of the collected ERT data with the acquired TEM soundings and resulting depth slices. In the *upper right corner* of the figure, a part of the altitude map (Fig. 3) of the area with the neighborhood TEM soundings and the acquired ERT profile is presented. The fracture zone between the dotted lines in the ERT profiles is depicted. The question marks show the uncertainty about the continuation of the fractures in depth. The bedrock in the ERT profile is composed of Tripolis limestones (T_3–K_2). The fracture zone dipping to the north is shown also by the geological symbol used in the altitude map. Since the ERT has good resolution to a depth of 94 m, the slices for the depths of 50–100 m, resulting from the 1D interpretation of the collected TEM data (*left part* of the figure), are included for simultaneous interpretation of the geophysical measurements. Finally, the resistivity log of the sounding A031 is also included over the ERT profile for evaluation and verification

configuration was applied incorporating topographic corrections. The system features 32 electrodes with 15-m electrode spacing (imaging depths of about 100 m depending on the subsurface resistivity), enabling fully automated measurements of the deep subsurface apparent resistivity. In total, 1,105 datum points (measurements) were acquired for the estimation of the final 2D tomographic model and after removing suspicious (bad quality, noisy) measurements, 975 data points remained for further processing (inversion) (Fig. 11).

The resistivity tomography data were processed and inverted using the commercial packages RES2DINV (Loke 1997). The 2D electrical signals were recorded and the final subsurface images were extracted during the inversion procedure. The high quality of the acquired data resulted in relatively low RMS (3.2%) errors for the inverted resistivity sections (Fig. 11). The final depth of penetration was 103 m, but based on the sensitivity and resolution matrix of the collected data file, the final inverted image reached a depth of 94 m below the surface.

In Fig. 11, the final inverted ERT profile in comparison with the TEM slices is presented. Based on the resolution of the inverted ERT data, the sensitivity of the model is high to a depth of 94 m and, therefore, the depth slices of TEM data to a depth of 100 m were selected for further combined interpretation. A fracture zone with an almost E–W direction can be easily identified (dotted lines in the ERT section) between the measurements A032 and north of A031 with an apparent thickness of about 225 m and dipping to north (see also relevant geological symbol in the altitude map). These characteristics (the existence of fracture zones and also the changes in resistivities) are in agreement with the depth slices of 50–100 m (Fig. 11, left part) and the 2D TEM section as presented in Fig. 6—

upper section. The resistivity log of the A031 sounding (black continuous line) is also presented over the ERT interpretation to verify the agreement between the resulting resistivity distribution.

The comparison between the 1D TEM results of A031 sounding, the ERT profile to a depth of 100 m, and the 2D and 3D imaging of the TEM data in the area confirm our proposed location of the suggested hydrowell for optimum exploitation of the study aquifer near the A031 sounding. Moreover, it shows that 1D survey can sufficiently image a complex (due to the tectonic) subsurface, but always supplementary methods should be used for verification of the resulting images/models.

Conclusions and recommendations

A detailed geoelectromagnetic survey was carried out acquiring more than 200 soundings in a grid of 100 points to reconstruct the 2D and 3D subsurface resistivity distribution. The detailed geo-electromagnetic survey in combination with the geological, tectonic and hydrolithological study of the area prior the geophysical campaign is a useful tool for the determination of the major hydrogeological characteristics of the area under investigation, as it can provide information on the geometrical and hydraulic information of the aquifer.

The survey managed to detect a shallow aquifer (conductor), which was detected in the course of the study. It seemed be of local extent, unconnected to the deeper one and a deep conductor (high-potential aquifer), the top of which was approximately 60 m below the surface and the thickness about 120 m. A 3D spatial distribution of formation resistivities was used for the identification of the main tectonic lines in the area close to the regions contaminated by saltwater intrusion (Figs. 8, 9). These fracture zones act as a barrier for the transport of freshwater to the sea and vice versa.

Beyond the results concerning the main objectives of the study, the presented work has shown that the TEM method is a practical, cost-effective technique for the hydrogeological delineation of coastal regions, even if no other geoenvironmental information are available for calibrating the model (such as, borehole logs). High-quality TEM data could be recorded near complex geological areas when the subsurface is conductive.

The following are recommended for future work at this location:

Due to geological complexity, 3D processing and inversion is also an essential point. It has to be applied by combining all the acquired TEM raw data of the study area. After that, the 3D modeling, which will be presented in depth slices covering the whole area, can be expected to be more reliable.

By individual inversion of the data, we showed that TEM and ERT methods are well suited to our area. Now, we should produce more tightly constrained interpretation models at several sites applying joint inversion of electrical and transient electromagnetic data.

Using the resistivity distribution in depth, we can estimate some hydraulic characteristics of the aquifer (Soupios et al. 2007), such as hydraulic conductivity and transmissivity. These data can be later used for simulating the groundwater flow and the interface of fresh/saline water.

Acknowledgments The authors are grateful to Dr. Elias Papadopoulos, Panayiotis Kanellopoulos, Panayiota Sarridou and Georgia Pegga, collaborators at TEI of Crete, for the great help during the TEM data acquisition. PS wishes to thank the Municipality of Souda and Ankara University in Turkey for partly supporting this work and Dr. K. Vozinakis (principal geologist of the Water Management Authority in Chania Prefecture) for the data provision and other useful information which help the completion of this work. This work is partially supported also by the project INTERREG IIIb, ARCHIMED, sub-project A1.020, MILDMAP: "Methodology integration of EO techniques as operative tool for land degradation management and planning in Mediterranean areas". We would also like to thank the reviewers for their constructive comments.

References

Albouy Y, Andrieux P, Rakotondrasoa G, Ritz M, Descloitres M, Join JL, Rasolomanana E (2001) Mapping coastal aquifers by joint inversion of DC and TEM soundings—three case histories. Ground Water 39:87–97

Alsharhan AS, Glennie KW, Whittle GL, Kendall CG (1998) Quaternary deserts and climatic change. Balkema Rotterdam. ISBN 9054105976

Athanasiou E, Tsourlos PI, Papazachos CB, Tsokas GN (2007) Combined weighted inversion of electrical resistivity data arising from different array types. J Appl Geophy 62(2):124–140

Auken E (1995) 1D time domain electromagnetic interpretations over 2D and 3D structures. In: Proceedings of the symposium on the application of geophysics to engineering and environmental problems. Orlando, USA. EEGS, pp 329–338

Barsukov PO, Fainberg EB, Khabensky EO (2007) Shallow investigation by TEM-FAST technique: methodology and case histories. In: Spichak VV (ed) Methods of geochemistry and geophysics. Elsevier, pp 55–77

Chalikakis K, Nielsen MR, Legchenko A (2008) MRS applicability for a study of glacial sedimentary aquifers in Central Jutland, Denmark. J Appl Geophys 66:176–187

Chartzoulakis KS, Paranychianakis NV, Angelakis AN (2001) Water resources management in the island of Crete, Greece, with emphasis on the agricultural use. Water Policy 3:193–205

Christensen NB (1995) 1D imaging of central loop transient electromagnetic soundings. J Environ Eng Geophys, pp 53–66

Christensen NB, Sørensen KI (1998) Surface and borehole electric and electromagnetic methods for hydrogeophysical investigations. Eur J Environ Eng Geophys 3(1):75–90

Danielsen JE, Auken E, Jørgensen F, Søndergaard VH, Sørensen KI (2003) The application of the transient electromagnetic method in hydrogeophysical surveys. J Appl Geophys 53:181–198

Drabbe J, Ghyben Badon W (1889) Nota in verband met de voorgenomen putboring nabij Amsterdam, Tijdschrift van het Koninklijk Instituut van Ingenieurs, 8–22

Duque C, Calvache ML, Pedrera A, Martín-Rosales VM, López-Chicano M (2008) Combined time domain electromagnetic soundings and gravimetry to determine marine intrusion in a detrital coastal aquifer (Southern Spain). J Hydrol 349:536–547

Fassoulas C, Kilias A, Mountrakis D (1994) Postnappe stacking extension and exhumation of high-pressure/low-temperature rocks in the Island of Crete, Greece. Tectonics 13(1):127–138

Fitterman DV, Labson VF (2005) Electromagnetic methods for environmental problems. In: Butler DK (ed) Near-surface geophysics. SEG Tulsa, Oklahama, pp 295–349

Goldman M, Gilad D, Ronen A, Melloul A (1991) Mapping of seawater intrusion into the coastal aquifer of Israel by the transient electromagnetic method. Geoexploration 28:153–174

Goldman M, Tabarovsky L, Rabinovich M (1994a) On the influence of 3-D structures in the interpretation of transient electromagnetic sounding data. Geophysics 59:889–901

Goldman M, Du Plooy D, Eckard M (1994b) On reducing ambiguity in the interpretation of transient electromagnetic sounding data. Geophys Prospect 42:3–25

Herzberg A (1901) Die Wasserversorgung einiger Nordsee bader, J. Gasbeleuchtung und Wasserversorgung, 44:815-819, 842-844

Hördt A, Scholl C (2004) The effect of local distortions on time domain electromagnetic measurements. Geophysics 68:87–96

Kafri U, Goldman M (2005) The use of the time domain electromagnetic method to delineate saline groundwater in granular and carbonate aquifers and to evaluate their porosity. J Appl Geophys 57:167–178

Kemna A, Nguyen F, Antonsson A, Engesgaard P, Tsourlos P (2006) Characterization of saltwater intrusion using electrical imaging: a numerical simulation study. In: Proceedings of 1st international joint salt water intrusion conference (SWIM-SWICA), Calgiari, Italy, 24–29 Sep 2006

Kocka S, Martini R, Reischmann T, Stampfli GM (2007) Detrital zircon and micropalaeontological ages as new constraints for the lowermost tectonic unit (Talea Ori unit) of Crete, Greece. Palaeogeogr Palaeoclimatol Palaeoecol 243(3–4):307–321

Loke MH (1997) Rapid 2D resistivity inversion using the least-squares method *RES2DINV Program Manual*. Penang, Malaysia

Macnae JC, Lamontagne Y, West GF (1984) Noise processing techniques for time domain EM systems. Geophysics 49:934–948

McCracken KG, Oristaglio ML, Hohmann GW (1986) The minimization of noise in electromagnetic exploration systems. Geophysics 51:819–832

Meju MA (1996) Joint inversion of TEM and distorted MT soundings: some effective practical considerations. Geophysics 61:56–65

Meju MA (1998) A simple method of transient electromagnetic data analysis. Geophysics 63:405–410

Meju MA, Fontes SL, Oliveira MFB, Lima JPR, Ulugergerli EU, Carrasquilla AA (1999) Regional aquifer mapping using combined VES-TEMAMTrEMAP methods in the semiarid eastern margin of Parnaiba Basin, Brazil. Geophysics 64:337–356

Newman GA, Anderson WL, Hohmann GW (1987) Interpretation of transient electromagnetic soundings over three-dimensional structures for the central-loop configuration. Geophys J R Astron Soc 89:889–914

Nielsen L, Jørgensen NO, Gelting P (2007) Mapping of the freshwater lens in a coastal aquifer on the Keta Barrier (Ghana) by transient electromagnetic soundings. J Appl Geophys 62:1–15

Papadopoulos NG, Tsourlos P, Papazachos C, Tsokas GN, Sarris A (2006) An algorithm for fast 3D inversion of parallel 2D ERT data-sets. In: 12th European Meeting of Environmental and Engineering Geophysics, Helsinki, Finland, 4–7 September 2006

Papadopoulos NG, Tsourlos P, Tsokas GN, Sarris A (2007) Efficient ERT Measuring and Inversion Strategies for 3D Imaging of Buried Antiquities. Near Surf Geophys 5(6):349–362

Papanikolaou D, Vassilakis E (2008) Middle Miocene E–W tectonic horst structure of Crete through extensional detachment faults. In: Donald D (ed) Harrington symposium on the geology of the Aegean, IOP conference series: earth and environmental science 2 012003. doi:10.1088/1755-1307/2/1/012003

Soupios P, Kouli M, Vallianatos F, Vafidis A, Stavroulakis G (2007) Estimation of aquifer parameters from surficial geophysical methods: a case study of Keritis Basin in Crete. J Hydrol 338:122–131

Strahler AN (1964) Quantitative geomorphology of basins and channel networks. In: Chow VT (ed) Handbook of applied hydrology. Mcgraw Hill Book Company, New York

Stummer P, Maurer H, Green AG (2004) Experimental design: electrical resistivity data sets that provide optimum subsurface information. Geophysics 69:120–139

TEM-RESearcher Manual (2007) Version 7. Applied Electromagnetic Research (AEMR), The Netherlands

Tsagarakis KP, Dialynas GE, Angelakis AN (2004) Water resources management in Crete (Greece) including water recycling and reuse and proposed quality criteria. Agric Water Manage 66:35–47

Tsourlos P, Ogilvy R (1999) An algorithm for the 3-D inversion of tomographic resistivity and induced polarisation data: preliminary results. J Balkan Geophys Soc 2:30–45

Tsourlos P, Athanasiou E, Kuras O, Wilkinson PB, Ogilvy RD (2006) Optimizing ERT measurements for hydrogeological monitoring: the case of Almeria (Spain). In: Proceedings, 12th annual meeting EAGE-near surface geophysics, Helsinki, Finland, September 2006

Tucker GE, Bras RL (1998) Hill slope processes, drainage density, and landscape morphology. Water Resour Res 34(10):2751–2764

Verruijt A (1968) A note on the Ghyben–Herzberg formula. Bull Int Assoc Sci Hydrol (Delft, Netherlands: Technological University) 13(4):43–46

Wilkinson PB, Meldrum PI, Chambers JE, Kuras O, Ogilvy RD (2006) Improved strategies for the automatic selection of optimized sets of electrical resistivity tomography measurement configurations. Geophys J Int 167:1119–1126